ARMY RESEARCH LABORATORY

Numerical Modeling of the Airborne Radar Signature of Dismount Personnel in the UHF-, L-, Ku-, and Ka-Bands

by Calvin Le and Traian Dogaru

ARL-TR-4336 December 2007

NOTICES

Disclaimers

The findings in this report are not to be construed as an official Department of the Army position unless so designated by other authorized documents.

Citation of manufacturer's or trade names does not constitute an official endorsement or approval of the use thereof.

Destroy this report when it is no longer needed. Do not return it to the originator.

Army Research Laboratory
Adelphi, MD 20783-1197

ARL-TR-4336 **December 2007**

Numerical Modeling of the Airborne Radar Signature of Dismount Personnel in the UHF-, L-, Ku-, and Ka-Bands

Calvin Le and Traian Dogaru
Sensors and Electron Devices Directorate, ARL

REPORT DOCUMENTATION PAGE

Form Approved
OMB No. 0704-0188

1. REPORT DATE *(DD-MM-YYYY)*	2. REPORT TYPE	3. DATES COVERED (From - To)
December 2007	Final	February to May 2007

4. TITLE AND SUBTITLE
Numerical Modeling of the Airborne Radar Signature of Dismount Personnel in the UHF-, L-, Ku-, and Ka-Bands

5a. CONTRACT NUMBER

5b. GRANT NUMBER

5c. PROGRAM ELEMENT NUMBER

6. AUTHOR(S)
Calvin Le and Traian Dogaru

5d. PROJECT NUMBER

5e. TASK NUMBER

5f. WORK UNIT NUMBER

7. PERFORMING ORGANIZATION NAME(S) AND ADDRESS(ES)
U.S. Army Research Laboratory
ATTN: AMSRD-ARL-SE-RU
2800 Powder Mill Road
Adelphi, MD 20783-1197

8. PERFORMING ORGANIZATION REPORT NUMBER
ARL-TR-4336

9. SPONSORING/MONITORING AGENCY NAME(S) AND ADDRESS(ES)
U.S. Army Research Laboratory
2800 Powder Mill Road
Adelphi, MD 20783-1197

10. SPONSOR/MONITOR'S ACRONYM(S)

11. SPONSOR/MONITOR'S REPORT NUMBER(S)

12. DISTRIBUTION/AVAILABILITY STATEMENT
Approved for public release; distribution unlimited.

13. SUPPLEMENTARY NOTES

14. ABSTRACT

This technical report presents numeric computations of the radar cross section (RCS) of a human body placed on top of a ground plane, as seen by an airborne radar. The simulated data was collected in four frequency bands, at low microwave frequencies (UHF- and L-bands), and high microwave frequencies (Ku- and Ka-bands). For the low frequency bands we used the Finite Difference Time Domain (FDTD) modeling technique, whereas for the high frequency bands we employed the Xpatch radar signature software. The results are presented as radar cross section (RCS) over a large range of azimuth and elevation angles. In general, we noticed a relatively small variation of the human body average RCS over a wide range of frequencies, spanning the interval from the UHF- to the Ka-band.

15. SUBJECT TERMS
Radar signature, computational electromagnetics

16. SECURITY CLASSIFICATION OF:			17. LIMITATION OF ABSTRACT	18. NUMBER OF PAGES	19a. NAME OF RESPONSIBLE PERSON
a. REPORT	b. ABSTRACT	c. THIS PAGE	UL	30	Traian Dogaru
Unclassified	Unclassified	Unclassified			19b. TELEPHONE NUMBER (*Include area code*) 301-394-1482

Standard Form 298 (Rev. 8/98)
Prescribed by ANSI Std. Z39.18

Contents

List of Figures

List of Tables

INTENTIONALLY LEFT BLANK

1. Introduction

The propagation of electromagnetic waves in the presence of the human body has been studied for a long time, related primarily to medical applications. During the 1990s, concerns about the health effects of electromagnetic radiation within the wireless industry prompted a number of studies trying to evaluate the radiation absorption rates inside the human body in the presence of an electromagnetic energy source. Most of those studies consisted of computer models of the wave propagation inside the body, and were made possible by advances in computer hardware, as well as the availability of mature electromagnetic (EM) simulation codes (*1 through 3*). The recent focus on military and national security applications, together with the emergence of the ultra-wideband (UWB) microwave radar as a promising technology for detecting the human presence in concealed environments, made the evaluation of the human body radar signature a problem of great interest. Reference (*4*) contains a detailed study of the human body radar signature, with emphasis on sensing through the wall applications. In that study, a ground-based radar scenario (handheld or vehicle borne) was assumed. However, not much information on the human body signature for airborne radar scenarios can be found in the literature. Furthermore, information on the human signature is even scarcer for frequencies higher than X-band. A practical scenario may actually involve a high degree of complexity, since we would also need to take into account the environment surrounding the human target (such as the ground plane), especially when the radar is operating at depression angles other than 0°.

Since the combinations of the various human shapes, postures and its environment are endless, numerical modeling of the human signature can prove very useful in designing and predicting the performance of a radar system for detecting human presence. Employing an exact EM solver is always the preferred choice for numerical simulations. However, even with the Department of Defense (DoD) state-of-the-art computing systems, using an exact EM code to predict the radar signatures for a large set of incidence angles at high frequencies is currently unfeasible. Therefore, for high frequency bands, we employ fast EM solvers that rely on various approximations that work well in those frequency regimes.

In this report, we examine the simulated radar cross section (RCS) of two standing men on a dielectric ground plane at various depression angles and azimuth aspect angles in the following frequency bands: UHF-band (0.3-0.5 GHz), L-band (1.2-1.5 GHz), Ku-band (15.2-18.3 GHz), and Ka-band (33.4-38.6 GHz). We also present a statistical characterization of the RCS data as a function of the radar orientation (azimuth angle), for various depression angles and polarizations. Finally, we discuss how these results compare with related measurement data.

2. Computational Approaches

Although in this study we are trying to simulate a simple scenario (the radar signature of a human body on top of a ground plane), there are multiple technical challenges in achieving this goal. First is the fact that the parameter space (frequency, aspect angle, polarization, the size and position of the human, etc.) is very large. Another important factor is represented by the ground plane electrical properties and degree of roughness, which have a significant impact on the radar return for depression angles other than 0°. Furthermore, we need fast and accurate numerical EM solvers that can handle targets as complex as the human body. In this context, the fidelity of the human computer-aided design (CAD) models that are suitable for the EM codes is critical for these applications.

In terms of modeling tools, we are leveraging the hardware and software infrastructure available to us at the U.S. Army Research Laboratory (ARL) and the DoD Major Shared Resource Centers (MSRC). The EM simulation software used in this work consists of the Finite Difference Time Domain (FDTD) and Xpatch. Although FDTD, an exact EM solver, would enable us to obtain accurate predictions at any frequencies, this technique is very computational intensive. Therefore, it is reasonable to run this code only in the lower frequency bands (UHF and L) for our problem. On the other hand, approximate solvers such as Xpatch, can provide the results in considerably less times and are more suitable for high frequencies and scenarios involving a large problem space. The following sections provide an overview of these two codes.

2.1 The Finite Difference Time Domain

The FDTD method is currently one of the most prominent techniques in electromagnetic wave modeling. Based on a relatively simple numerical scheme, FDTD benefited from the spectacular advances in computer hardware and architecture, as well as the intense research activity in the field of computational electromagnetics (CEM), to become a mainstream modeling technique for wave phenomena in the 1990s. The literature dedicated to FDTD is mature, and there are a number of reference books containing a comprehensive treatment of the subject (*5,6*). In this section, we will summarize a few important aspects of this numerical technique.

The FDTD algorithm is based on discretizing Maxwell's time-domain equations, using finite differences in spatial and temporal dimensions. The computational space, with a uniform, rectangular, grid-like structure, is made of elementary cubic cells. The electromagnetic field components are computed along the cell's edges and faces, at discrete time steps. Each cubic cell is assigned the material properties (permittivity ε, permeability μ, and conductivity σ) of the corresponding region in space. By discretizing Maxwell's equations in time and space, we obtain the so-called FDTD update equations, which allow the updating of a current field component sample, based on the values of neighboring field component samples obtained at a

previous time step. FDTD can handle almost arbitrary media electric properties and geometries. The geometry implementation is relatively simple (at least in the most basic implementation form), and there are very few restrictions on topologies, relative positions of targets and ground planes, as well as mixing various materials inside targets or grids. Since FDTD operates in the time domain, results can be provided over a wide range of frequencies in one time-marching run, at any angle of observation. This is ideal in simulating the operation of a short-pulse UWB radar. In terms of programming, the core of the algorithm (the update equations) is easy to implement. Also, the algorithm is an excellent candidate for parallelization, which allows the user to take advantage of the huge computing power available at high performance computing (HPC) centers.

The main disadvantage of FDTD is its computational expense: the computational space increases very rapidly with the wave frequency (f). Thus, the memory used by the code increases with f^3, whereas the central processing unit (CPU) time increases with f^4. This is related to the need to spatially oversample the fields in order to mitigate the numerical dispersion (*5*). In general, Xpatch can achieve vastly superior speed in modeling the same problem as FDTD (typically 100 to 1000 times faster).

There are many applications and many available implementations of the FDTD algorithm. The code we used for this work is called AFDTD, and was entirely developed at ARL for radar signature modeling. This is a parallel code for distributed systems, specialized in solving far-field radar scattering problems in a half-space environment (that is, including a dielectric ground plane). AFDTD can import meshes and output data in various formats, compatible with other popular CEM codes. The AFDTD code was run at the U.S. Army MSRC (*7*), on Linux Networx Evolocity II clusters. The graphics in this report were done with Matlab and Pioneer RCS. The pre- and post-processing were performed on Dell workstations running Windows XP.

2.2 Xpatch

Xpatch is a powerful CEM code, designed specifically to compute and analyze radar signatures at high frequencies (*8*). It was developed by Science Applications International Corporation (SAIC), under a grant from the U.S. Air Force. It is currently an export controlled software package, available only to U.S. government users or DoD contractors. A number of papers have been published in the open literature (e.g., (*9 through 11*)), presenting modeling results obtained with Xpatch. Moreover, the radar signature modeling group at ARL has successfully used Xpatch in simulating the radar return from various targets, including human body (*12*), rooms and buildings (*12*), military vehicles (*13 through 16*), at frequencies ranging from L- to Ka-band.

Xpatch is part of a family of CEM techniques that rely on high-frequency approximations to model field propagation and scattering. In particular, it implements ray tracing combined with physical optics (PO) (*17*) to compute the radar return from arbitrary targets. The code has a powerful built-in graphics user interface (GUI), which allows the user to draw and analyze complex meshes, and visualize the data. Xpatch is coupled with other SAIC-proprietary

software packages, both for various mesh conversions and manipulations (ModelMan, XEdge), and for data visualization (Pioneer RCS, XYPlot). In the applications presented here, the meshes describe the target surface, using a triangular facet model.

Although Xpatch has been successfully used in a large number of radar applications, it has a number of limitations, which stem from the approximate nature of the methods it implements. Thus, the PO approximation may produce wrong results at angles off the specular direction, and cannot accurately account for diffraction off dielectric wedges. Also, it does not capture important wave phenomena, such as surface, creeping or traveling waves, as well as some interesting effects in multiple scattering scenarios. Other limitations may come from the target representation as a triangle facet model. Generally, for higher frequencies we must use a smaller facet size to describe the same target, which increase the simulation time.

The Xpatch simulations presented in this report were performed at ARL, on Dell Linux workstations, as well as HPC Linux Networx Evolocity II clusters at the DoD MSRC centers.

3. Numerical Results

3.1 The CAD Models

For the human body modeling we used two different meshes, described in figures 1 and 2. The FDTD models use the mesh in figure 1 (that we call the "fat man"), which we found on a website maintained by the U.S. Air Force Research Laboratory, RF Radiation Branch (Brooks Air Force Base) (*18*). (Unfortunately, the page containing the human body models is no longer available.) The meshes stored at this site represented highly detailed FDTD-compatible grids, where the dielectric properties of each human tissue are sampled using 1 mm, 2 mm, or 3 mm cubic cells. Tables containing the complex permittivities of the tissues as parametric functions of frequency were provided in reference (*19*). In this study, the computational grid has a 3 mm resolution, which is more than sufficient for frequencies up to L-band. More details on the specific computational grid used by the AFDTD code can be found in reference (*4*). The mesh in figure 2 (that we call the "fit man"), made of triangular facets, was used with the Xpatch models. This mesh was built by manipulating a CAD model of the human body that we obtained from a commercial website (*20*). Since this model does not include the internal structure of the body, but only the exterior shell, we must assume that the entire body is made of the same uniform dielectric material. For this material we picked dielectric properties close to those of skin, with complex permittivity $\varepsilon_r = 50 - j12$.

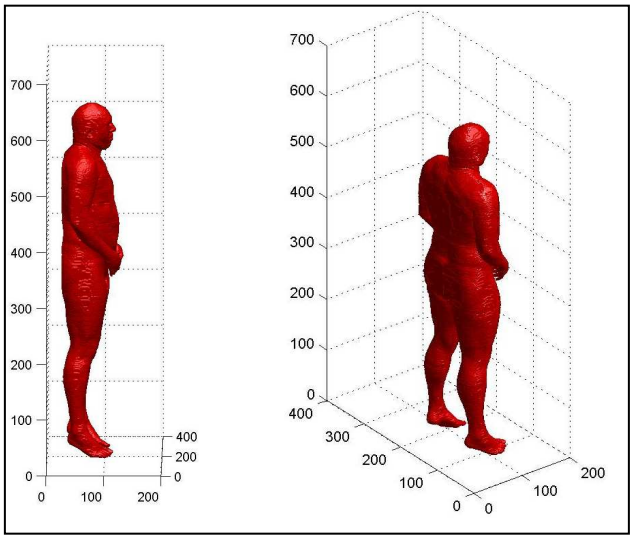

Figure 1. Three-dimensional FDTD grid for the "fat man" body model.

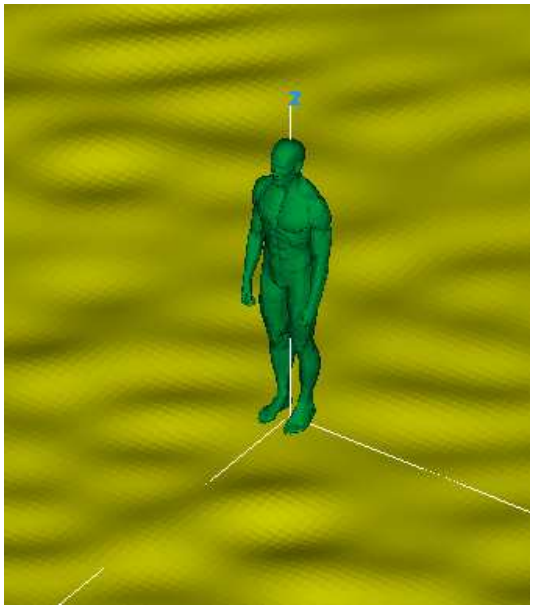

Figure 2. Triangle facet model of the "fit man" standing on top of a rough ground plane, used in the Xpatch simulations.

In both cases we added a dielectric ground plane, which is essential in building a realistic model for an airborne radar system. For the FDTD model, the ground has $\varepsilon_r = 10$, $\sigma = 0.05$ S/m, whereas for the Xpatch model we used a complex ground permittivity of $\varepsilon_r = 10 - j$ (the differences come from implementation-specific issues with the two simulation computer codes). Moreover, for the Xpatch model we introduced a slight ground roughness, with Gaussian distribution and Gaussian spectrum, exhibiting a root mean square (RMS) height of 0.5 in. and a correlation length of 6 in.

3.2 FDTD Modeling

The computational domain for the "fat man" was made of $233 \times 495 \times 612$ cells with a 3 mm resolution. Since we are interested in RCS-type calculations, the sources and receivers are assumed in the far field.

One important question was related to the validity of the uniform dielectric body model, such as the "fit man" used in the Xpatch simulations. In order to answer this question, we compared the RCS of the "real" model to that of a man made of a uniform material with dielectric properties close to the skin. At $\varepsilon_r = 50$, $\sigma = 1$ S/m, this material acts almost as a perfect reflector, so penetration of the radar waves through the body should not play a significant role in the RCS in this case. We show the vertical-vertical (V-V) polarization RCS plots for the two scenarios in figure 3 (a free-space environment and a 0° depression angle were used in this simulation). Looking at the two graphs, we concluded that, except for low frequencies (up to 1.2 GHz), there are essentially no differences in the radar signature between the two models. However, as expected, the lower frequencies do penetrate the thin layer of skin and hit a relatively low dielectric/loss fat tissue, bouncing back and creating interference. Therefore, at low frequencies, the internal body structure could play an important role in determining the radar return. In consequence, we used the full human body model for all the FDTD simulations, which extend up to 1.5 GHz. However, for higher frequencies, the uniform dielectric body model offers a very good approximation in terms of evaluating the RCS. This justifies our approach in using the uniform dielectric body model with Xpatch in the Ka- and Ku-bands.

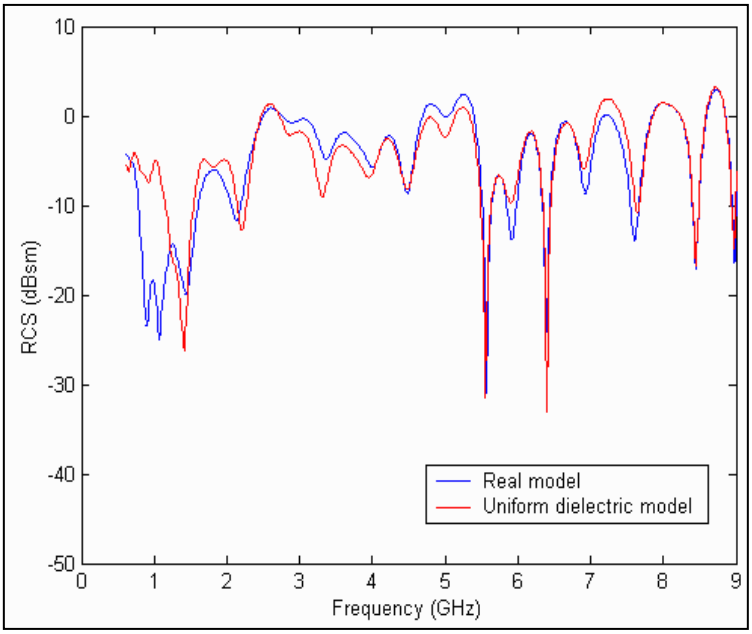

Figure 3. RCS comparison between the complete fat man body model and a body model with identical geometry, but made of a uniform dielectric material (with 0° azimuth (front view) at 0° elevation and V-V polarization).

The RCS of the "fat man" on a flat dielectric ground was calculated at 0°, 15°, 30°, 45°, and 60° depression angles. The depression angle here is defined as the angle measured from the ground plane. Due to symmetry, simulations were performed only from 0° to 180° azimuth, for every 1° step angle. Although we obtained simulation results for frequency up to 3 GHz, only the frequency bands of interest were extracted below. In the following graphs, we plot the average RCS over the frequency band of interest—that is, we compute the linear average of the RCS values obtained for a number of data points at equally spaced discrete frequencies within that band. For instance, in the UHF-band (0.3-0.5 GHz) we used 32 frequency data points, whereas in the L-band (1.2-1.5 GHz) we used 48 frequency data points.

Figure 4a shows the average RCS in the UHF-band as a function of azimuth angle for 0° depression, where the ground plane does not play a role in the radar scattering return. Incidence at 180° azimuth corresponds to a view from the back, and we notice a relatively large RCS and slow variation with the angle in this azimuth range. This is because the "fat man's" back has a very flat shape and produces a strong radar return in the backscattering direction. Except near the backside view angles, the average RCS in this band does not vary much across the azimuth angles, with no more than approximately 5 dBsm difference between the minimum and maximum values for both polarizations. This characteristic changes drastically in the L-band. As shown in figure 4b, the variation of the average RCS is much more rapid—the values may swing as much as 10 dB within less than 10° of displacement. In this case, as the target size is increased with respect to the wavelength, the target details start to have a significant impact on the radar return. Notice that, in both frequency bands, the RCS of both polarizations (V-V and H-H) are very similar at 0° depression angle.

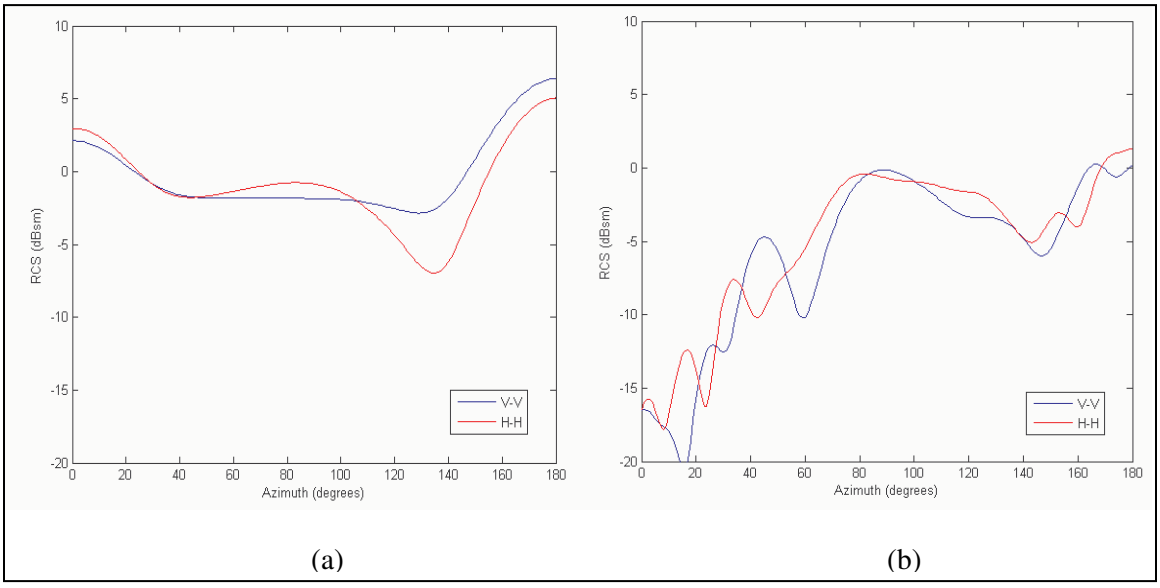

Figure 4. RCS of the fat man versus azimuth angle at 0° depression angle in the (a) UHF-band and (b) L-band.

For other elevation angles, the RCS is strongly dependent on the polarization as shown in figures 5 through 8. With the exception of a few azimuth angles, the radar scattering return in the H-H polarization is much stronger than in V-V polarization. This trend is observed for both frequency bands. This phenomenon can be explained by the fact that the ground bounce of the radar waves, which plays an important role in the backscatter return, is more prominent in H-H than in V-V polarization (this effect can be linked to the existence of the Brewster angle for V-V polarization only (*17*)). Thus, the ground plane is definitely a factor in enhancing the human RCS, especially in the H-H polarization. Table 1 shows the FDTD-computed frequency-average RCS of the "fat man" averaged across 180° of azimuth angles as well. It should be emphasized that the numbers in the table are characteristic to one human shape, one posture, and one set of dielectric ground plane properties. However, the numerical models in reference (*4*) suggest the fact that the average RCS of the human body is not very sensitive to the body shape and posture. Table 1 summarizes the average RCS values computed across frequency and all azimuth angles, at the depression angles mentioned above, in the UHF- and L-bands.

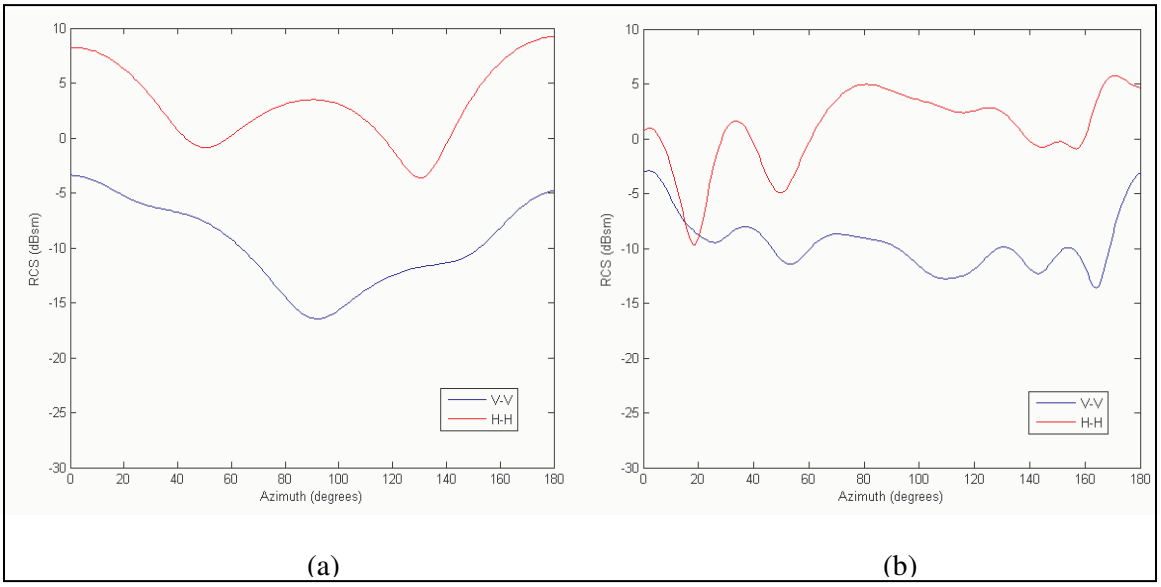

Figure 5. RCS of the fat man versus azimuth angle at 15° depression angle in the (a) UHF-band and (b) L-band.

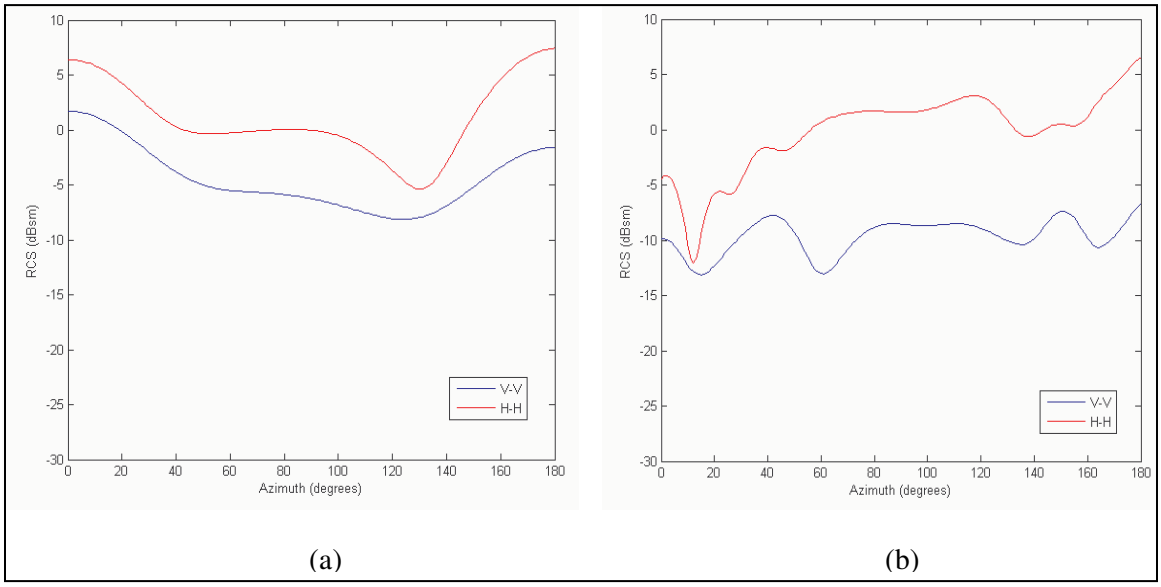

Figure 6. RCS of the fat man versus azimuth angle at 30° depression angle in the (a) UHF-band and (b) L-band.

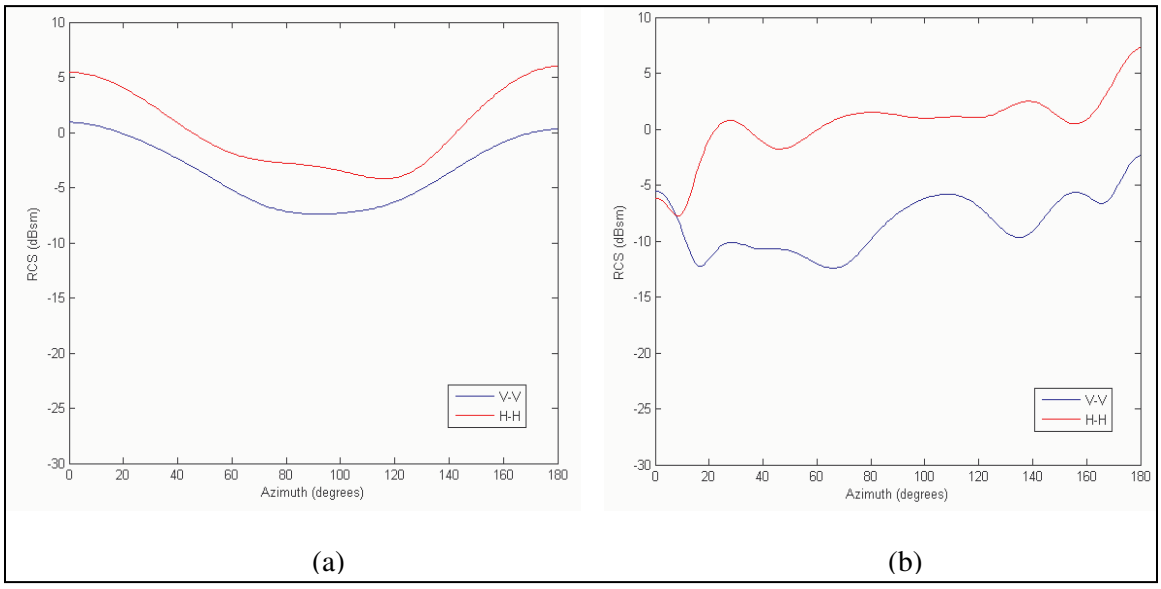

Figure 7. RCS of the fat man versus azimuth angle at 45° depression angle in the (a) UHF-band and (b) L-band.

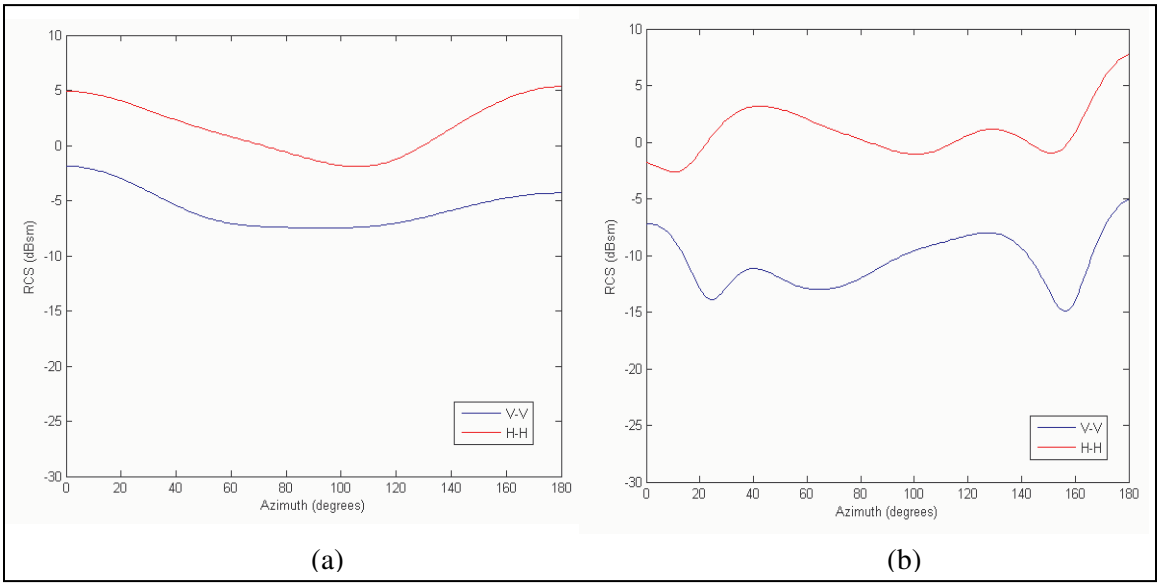

Figure 8. RCS of the fat man versus azimuth angle at 60° depression angle in the (a) UHF-band and (b) L-band.

Table 1. The fat man average RCS over frequency and azimuth angle in the UHF- and L-bands.

Depression Angle		**0°**	**15°**	**30°**	**45°**	**60°**
UHF-Band	V-V	0.63	–8.17	–3.45	–2.65	–5.30
	H-H	–0.04	4.40	2.36	1.59	2.25
L-Band	V-V	–3.51	–8.73	–9.40	–7.77	–9.97
	H-H	–3.06	2.02	0.96	1.21	1.56

3.3 Xpatch Modeling

As mentioned above, running an exact electromagnetic model in the Ku- and Ka-frequency bands is a very computationally intensive task. Our approach was to use the Xpatch code in order to obtain a fast solution. Since the code is based on the shooting and bouncing ray technique, the most time consuming process during a run is the ray tracing part. Once the ray paths are determined, the PO-based scattered fields can be computed for all frequencies of interest very rapidly. The density of shooting rays, which is defined in term of rays per wavelength, is typically set at 10 rays per wavelength for the highest frequency in order to obtain an accurate solution. To make sure that this ray density is sufficient for our problem, we did a convergence study, in which we pushed this number upward to 30 rays per wavelength with no noticeable change in the results for several depression angles.

An important issue that we needed to address was the validity of the Xpatch human body radar signature models, given the fact that Xpatch is based on approximations in the electromagnetic scattering theory. We investigated this issue in reference (*12*), by comparing the radar signature of the human body as computed with Xpatch and FDTD below 3 GHz, with satisfactory results.

In that report, we converted the triangular facets of the "fit man" model to cubic cell FDTD grid using our in-house converter software, as presented in figure 9. Figure 10 shows the results of the comparison at 3 GHz for the "fit man" model at 0° depression angle. For the front or back view, the human body has more of a flat surface aspect and this is where Xpatch yields the most accurate results. For the side view, the surface seen by the radar is smaller and has more curvature—these are cases that are handled by Xpatch with less accuracy due to the PO approximation limitations. However, the overall agreement is quite good. Although we were not able to run this validation in the Ku- and Ka-bands (because of computational space limitations with the FDTD code), we expect the Xpatch accuracy to improve at higher frequencies, where the code was originally designed to work.

Given the efficiency of running Xpatch simulations, we were able to generate a large data set for the "fit man" model on a slightly rough dielectric ground plane at Ku- and Ka-bands. This scenario simulates a human standing on a surface other than man-made smooth surfaces such as concrete floor, asphalt road, etc. A slight roughness in the ground plane might appear small at low frequencies (where it can be treated as a flat surface), but not so in the high frequency regime.

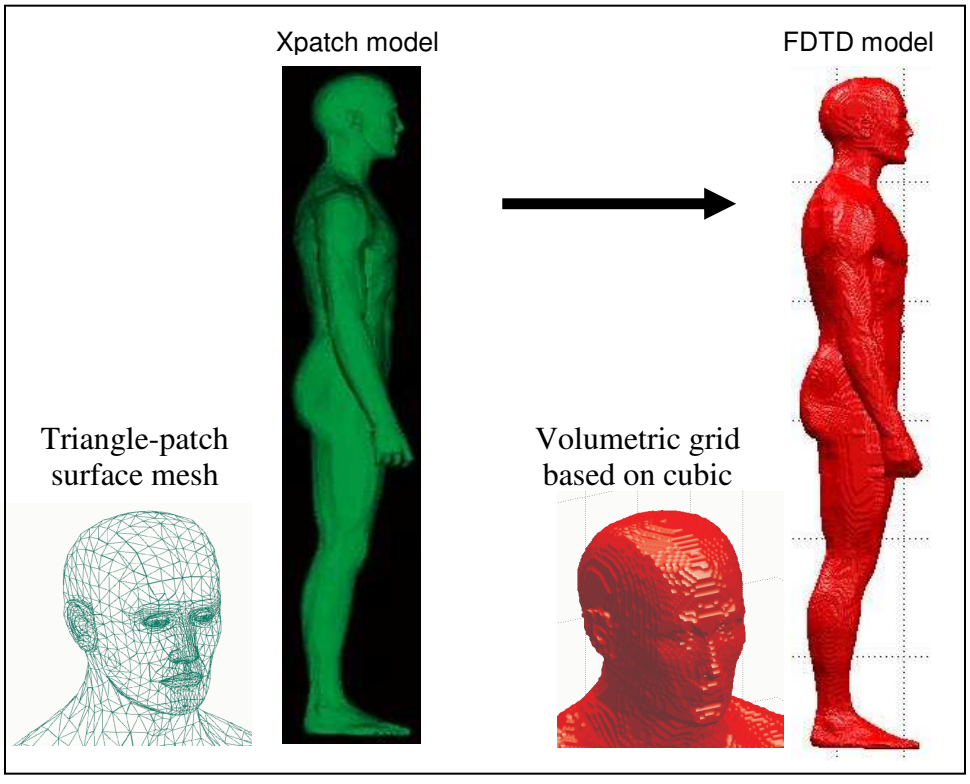

Figure 9. The mesh conversion process from triangle-patch model to cubic cell volumetric grid, used in comparing the Xpatch and FDTD models of the human radar signature (*12*).

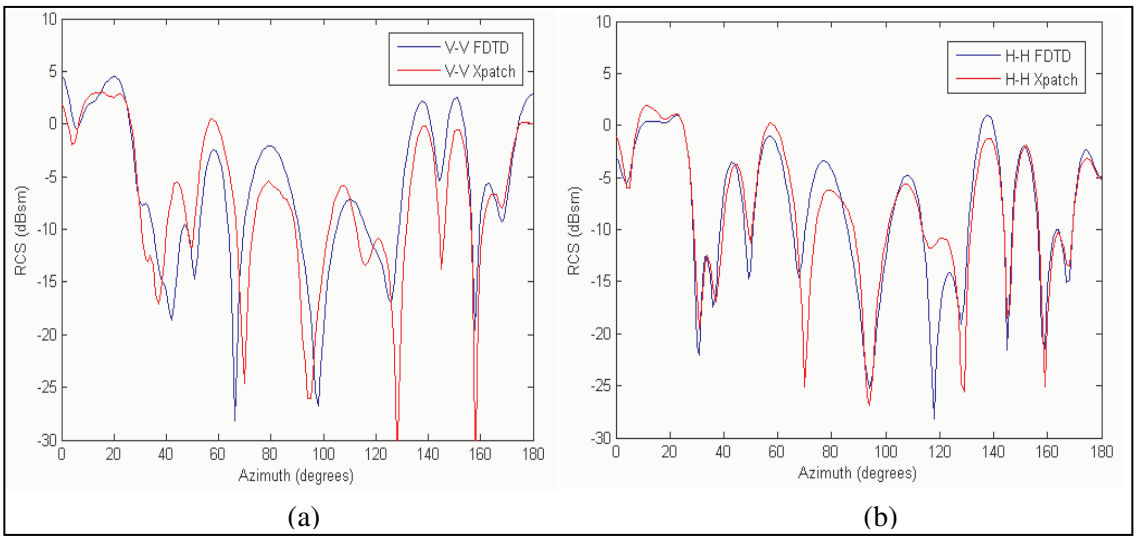

Figure 10. Comparison between Xpatch and FDTD for the fit man at 3 GHz and 0° depression angle, showing the RCS versus azimuth angle for (a) V-V polarization and (b) H-H polarization.

Figure 11 shows the average RCS versus the azimuth angle, at 0.5° intervals, for both frequency bands and polarizations, at 0° degree depression angle. The RCS variation is more rapid than at L-band frequencies since the target size is now electrically much larger, and the details in the body parts become a very important factor. This fluctuating behavior is consistent with available measurement data of a pedestrian at 76 GHz (*21*). This further confirms the validity of using Xpatch for human modeling in the high frequency bands. Without the ground effects, there is not much difference in the human radar signature for the two polarizations, which is consistent with our observations in the lower frequency bands.

At higher depression angles, the RCS in H-H polarization is again higher as compared to the V-V polarization. Illustrated in figure 12 is the RCS return at 30° degree depression angle. Notice in figures 11 and 12 that the RCS versus azimuth angle has the same trend in both frequency bands. The results at other depression angles share the same behavior as the results for 30°. In order to provide an overall picture of the RCS variation across the entire incidence angle spectrum, we mapped the average RCS into a polar plot format for the Ku- and Ka-bands in figure 13. These plots were generated between 0° and 60° depression angles, with 5° steps, and between 0° and 180° azimuth angles, with 0.5° steps. In each plot, the RCS variation is less than 10 dB over the entire angular spectrum for each polarization. Comparing the RCS maps in figure 13, for both polarizations, we notice that they look very similar, leading to the conclusion that the RCS value does not change much with frequency. This phenomenon is consistent with what we observed in other studies, regarding both simulated and measured data for ground targets in the X-band and Ka-band (*14,15*). Tables 2 and 3 provide the overall statistic RCS data of the "fit man" in the Ku- and Ka-bands, respectively.

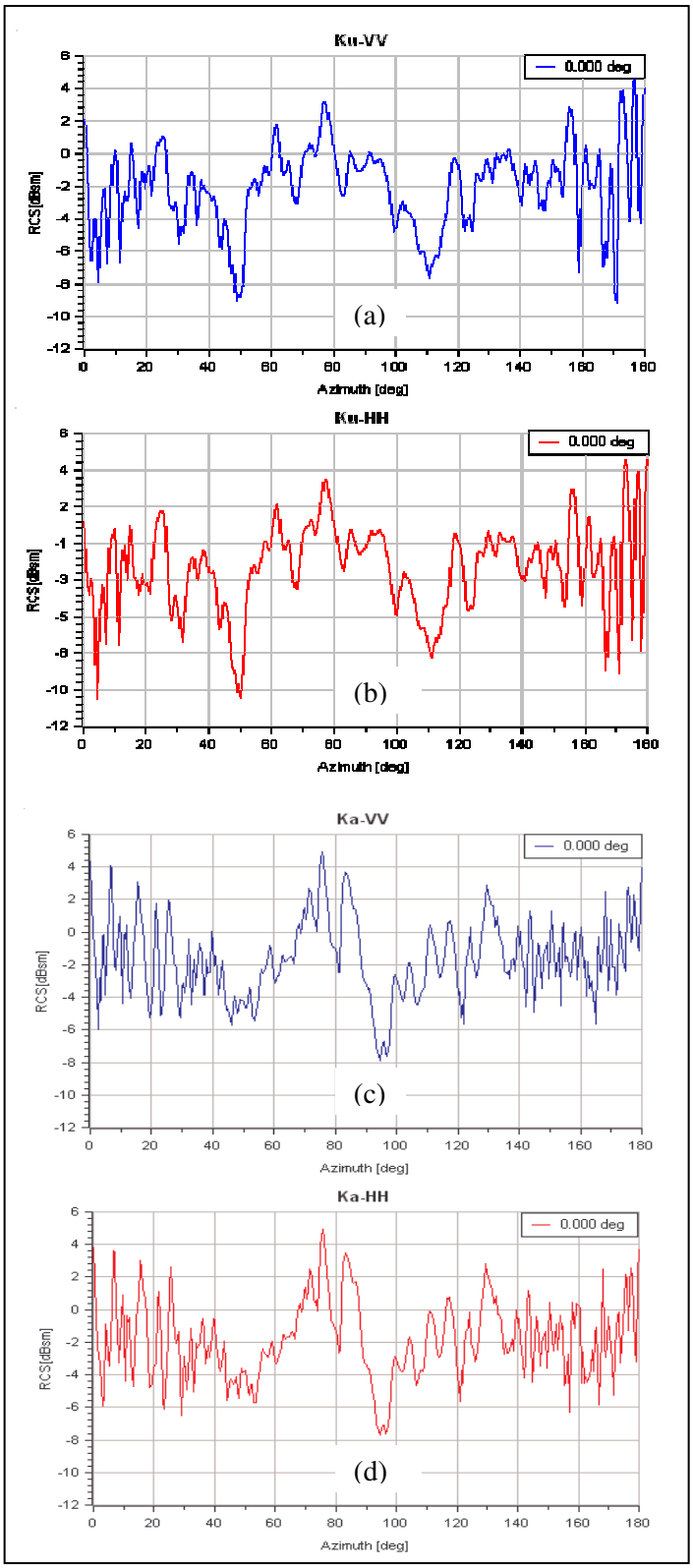

Figure 11. RCS of the fit man versus azimuth angle at 0° depression angle for: (a) Ku-band, V-V polarization; (b) Ku-band, H-H polarization; (c) Ka-band, V-V polarization; (d) Ka-band, H-H polarization.

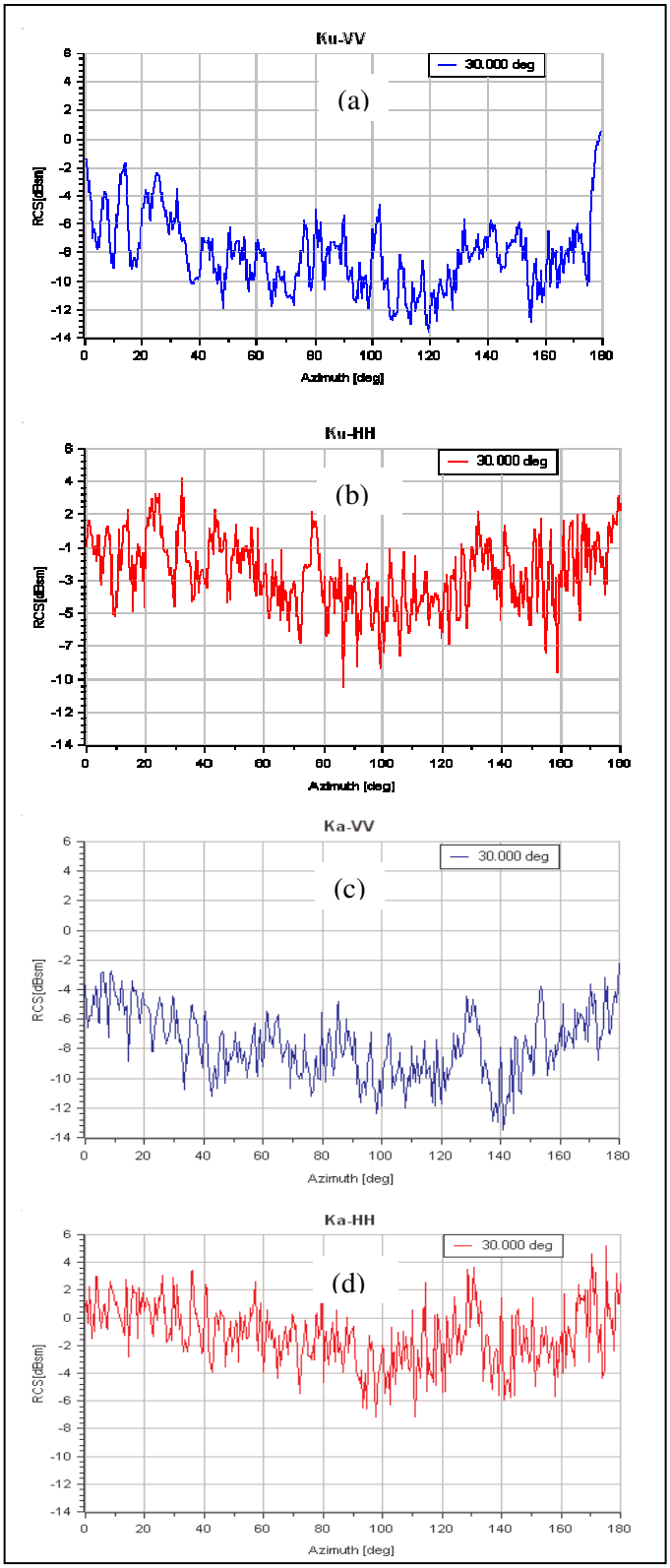

Figure 12. RCS of the fit man versus azimuth angle at 30° depression angle for: (a) Ku-band, V-V polarization; (b) Ku-band, H-H polarization; (c) Ka-band, V-V polarization; (d) Ka-band, H-H polarization.

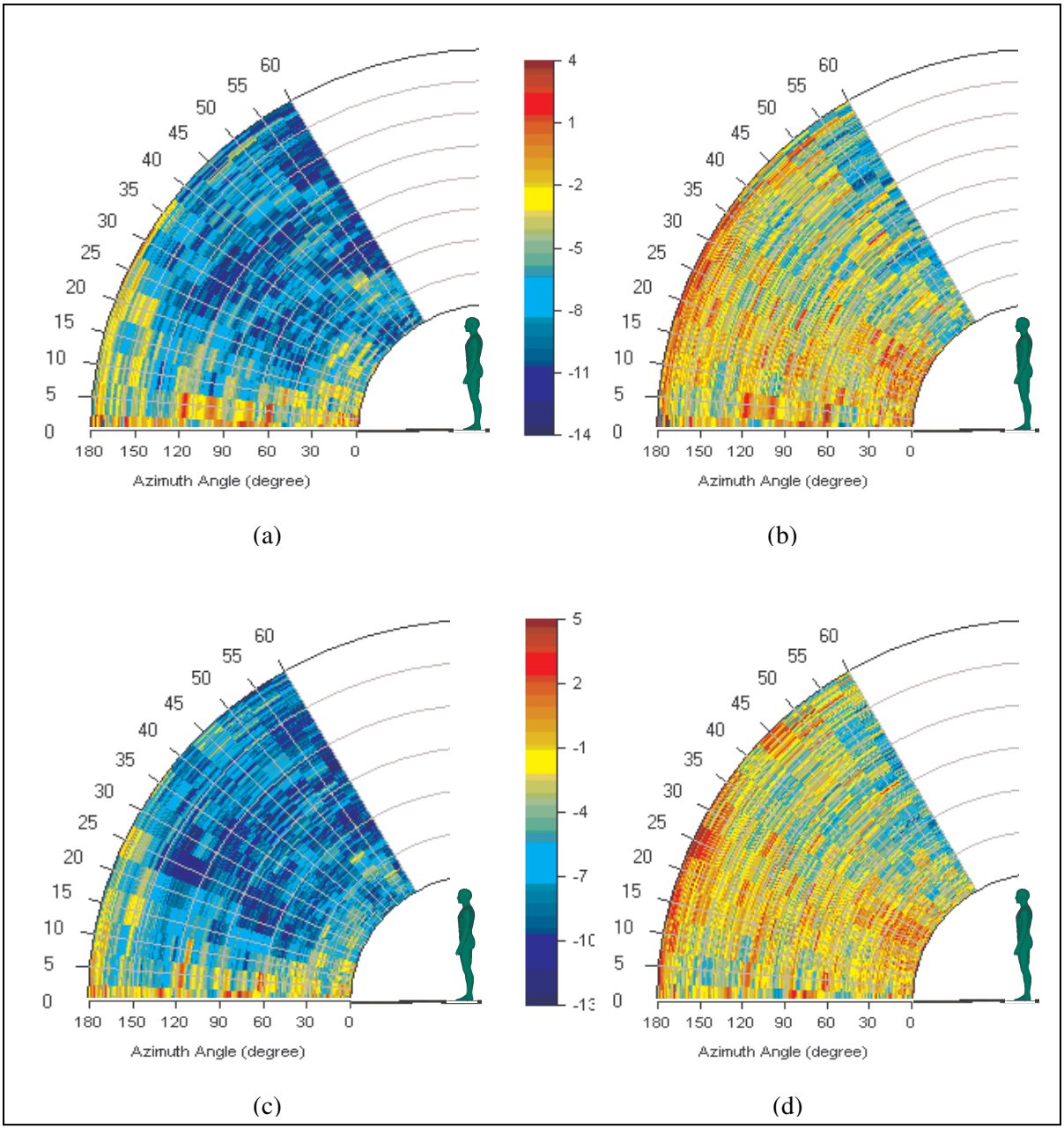

Notes: The scale in the elevation dimension represents the depression angle in degrees. The intensity scales are in dBsm.

Figure 13. Polar plot of the frequency-average RCS of the fit man for: (a) Ku-band, V-V polarization; (b) Ku-band, H-H polarization; (c) Ka-band, V-V polarization; (d) Ka-band, H-H polarization.

Table 2. Statistical RCS data for the fit man in the Ku-band.

Depression Angle		**0°**	**5°**	**10°**	**15°**	**20°**	**25°**	**30°**	**35°**	**40°**	**45°**	**50°**	**55°**	**60°**
Mean (dBsm)	W	–2.1	–3.1	–5.1	–5.6	–7.1	–7.8	–8.1	–8.5	–8.8	–8.7	–8.1	–9.3	–10.2
	HH	–2.2	–2.3	–2.5	–2.1	–2.1	–2.1	–2.4	–3.5	–4.2	–4.2	–3.9	–5.7	–6.4
Median (dBsm)	W	–1.6	–3.0	–4.7	–5.9	–7.5	–8.4	–8.2	–8.6	–8.7	–8.6	–8.1	–9.4	–10.4
	HH	–1.8	–2.3	–2.4	–2.0	–1.9	–2.3	–2.4	–3.7	–4.3	–4.2	–3.9	–5.8	–6.4
Standard deviation (dBsm)	W	2.6	2.3	2.3	2.1	2.5	2.7	2.6	2.5	1.8	2.1	2.4	2.3	1.9
	HH	2.7	2.2	1.9	1.8	1.9	2.3	2.5	2.3	2.0	2.0	2.5	2.3	2.3

Table 3. Statistical RCS data for the fit man in the Ka-band.

Depression Angle		**0°**	**5°**	**10°**	**15°**	**20°**	**25°**	**30°**	**35°**	**40°**	**45°**	**50°**	**55°**	**60°**
Mean (dBsm)	W	–1.6	–3.0	–4.7	–5.5	–7.1	–7.8	–7.8	–7.6	–7.9	–7.7	–7.3	–8.2	–9.1
	HH	–1.8	–2.0	–1.7	–1.0	–0.9	–0.6	–1.2	–2.2	–3.0	–3.0	–2.9	–3.9	–4.7
Median (dBsm)	W	–1.7	–3.2	–4.7	–5.8	–7.0	–8.5	–7.9	–7.8	–7.8	–7.7	–7.3	–8.5	–9.1
	HH	–2.0	–2.0	–1.7	–1.0	–1.0	–0.7	–1.3	–2.3	–3.0	–3.1	–3.0	–3.9	–4.8
Standard deviation (dBsm)	W	2.4	2.2	2.0	2.2	2.2	3.0	2.2	2.2	1.8	2.0	2.2	2.4	2.1
	HH	2.4	2.0	1.8	1.8	1.7	2.2	2.2	2.0	2.0	2.2	2.2	2.1	2.4

4. Conclusions

We have conducted a fairly thorough investigation in modeling the signature of a human body on top of a dielectric ground plane, as seen by an airborne radar at various depression angles. Knowing the expected strength and variability of the radar return from a human is a valuable piece of information for the radar system designer. In this study, we used both an exact EM solver (FDTD), and an approximate code (Xpatch). We covered the entire range of azimuth angles, in the UHF-, L-, Ku-, and Ka-frequency bands, for both V-V and H-H polarizations. As we have shown in previous studies, Xpatch can provide satisfactory results, while being on the order of 100 to 1000 times faster than FDTD. This makes us confident in using Xpatch to predict the radar signature of a human body in the higher frequency bands.

At 0° depression angle, the average RCS for both V-V and H-H polarizations are very similar. The RCS values are typically higher around the cardinal angles (0°, 90°, 180°, and 270°), where the target exhibits less curved surfaces in the specular direction. For other azimuth angles, the RCS variation is small in the UHF band (less than 5 dBsm), and less than 10 dBsm for all the other frequency bands of interest. Looking at the human body average RCS (over both frequency and azimuth angle) we notice that it varies in a tight range (from –3.5 to 0 dBsm) across all frequency bands of interest.

For depression angles other than 0°, the RCS return for the H-H polarization is always higher than the V-V polarization due to ground effects, for both the flat and slightly rough dielectric ground plane models. The differences are dependent upon the depression angle, ground characteristics, and radar frequency. For frequencies in the L-band and below, the average RCS values are from –10 to –3 dBsm for V-V polarization, and 1 to 4 dBsm for H-H polarization. For frequencies in the Ku-band and above, the average RCS values are from –10 to –3 dBsm for V-V polarization, and –6 to 0 dBsm for H-H polarization. Notice that the difference in RCS values between polarizations is larger for the low frequency bands, where we used the flat ground plane model. In other words, the enhancement in the human RCS due to the ground plane is smaller in the case of a rough ground plane, since the roughness introduces a loss of coherence in the ground bounce. This highlights the important of selecting an appropriate ground surface model for high frequency bands.

5. References

1. Lazzi, G.; Pattnaik, S.; Furse, C.; Gandhi, O. Comparison of FDTD Computed and Measured Radiation Patterns of Commercial Mobile Telephones in Presence of the Human Head. *IEEE Transactions on Antennas and Propagation* **June 1998**, *46*, 943-944.

2. Tinniswood, A.; Furse, C.; Gandhi, O. Computations of SAR Distributions for Two Anatomically Based Models of the Human Head Using CAD Files of Commercial Telephones and the parallelized FDTD code. *IEEE Transactions on Antennas and Propagation* **June 1998**, *46*, 829-833.

3. Toftgard, J.; Hornsleth, S.; Andersen, J. Effects of Portable Antennas in the Presence of a Person. *IEEE Transactions on Antennas and Propagation* **June 1993**, *41*, 739-746.

4. Dogaru, T.; Nguyen, L.; Le, C. *Computer Models of the Human Body Signature for Sensing Through the Wall Radar Applications*; ARL-TR-4290; U.S. Army Research Laboratory: Adelphi, MD, September 2007.

5. Taflove, A.; Hagness, S. C. *Computational Electrodynamics: The Finite-Difference Time-Domain*; Artech House, Boston, MA, 2000.

6. Kunz, K.; Luebbers, R. *The Finite-Difference Time-Domain Method for Electromagnetics*; CRC Press, Boca Raton, FL, 1993.

7. ARL MSRC Web page. http://www.arl.hpc.mil (accessed August 2007).

8. XPATCH User's Manual, SAIC/DEMACO, Champaign, IL. This document is export controlled, available to U.S. Government users and DoD Contractors only.

9. Andersh, D.; Hazlett, M.; Lee, S.; Reeves, D.; Sullivan, D.; Chu, Y. Xpatch: A High-Frequency Electromagnetic Scattering Code and Environment Prediction for Complex Three-Dimensional Objects. *IEEE Antennas and Propagation Magazine* **February 1994**, *36*, 65-69.

10. Andersh, D.; Lee, S.; Moore, J.; Sullivan, D.; Hughes, J.; Ling, H. Xpatch Prediction Improvements to Support Multiple ATR Applications. *Proceedings of SPIE*, Orlando, FL, *3395*, 108-119, 1998.

11. Andersh, D.; Moore, J.; Kosanovich, S.; Kapp, D.; Bhalla, R.; Kipp, R.; Courtney, T.; Nolan, A.; German, F.; Cook, J. Xpatch 4: The Next Generation in High-Frequency Electromagnetic Modeling and Simulation Software. *The Record of the IEEE 2000 International Radar Conference*, Alexandria, VA, 844-849, May 2000.

12. Dogaru, T.; Chamma, W.; DiFilippo, D.; Biggs, R. *Through-the-Wall Radar EM Modeling Techniques and Validation*; TTCP SEN TP3 Technical Report, Sept. 2007.

13. Spurgeon, W. A.; Hopkins, D. A. *An Xpatch Study of the T5M3 Simulator and Three Simpler Variants*; ARL-TR-2851; U.S. Army Research Laboratory: Adelphi, MD, September 2002.

14. Coburn, W. O.; Le, C. *An Investigation of the ZSU-23-4 Radar Cross Section at X-Band*; ARL-TR-3003; U.S. Army Research Laboratory: Adelphi, MD, June 2003.

15. Coburn, W. O.; Le, C. *A Numerical Study of the ZSU-23-4 and T72M1 Ka-Band Radar Signature*; ARL-TR-3325; U.S. Army Research Laboratory: Adelphi, MD, September 2004.

16. Dogaru, T.; Le, C. *Xpatch and FDTD Modeling of the M1 Tank Radar Signature in the L-Band*; ARL-TR-4291; U.S. Army Research Laboratory: Adelphi, MD, September 2007.

17. Knott, E.; Shaeffer, J.; Tuley, M. *Radar Cross Section*; Artech House, Boston, MA, 1993.

18. Brooks Air Force Base Web page. http://www.brooks.af.mil (accessed September 2003).

19. Gabriel, C. *Compilation of the Dielectric Properties of Body Tissue at RF and Microwave Frequencies*; USAF School Aerospace Med., Brooks AFB, TX, AL/OE-TR-1996-0037, 1996.

20. 3D CAD Browser Web page. http://3dcadbrowser.com (accessed July 2005).

21. Yamada, N.; Tanaka, Y.; Nishikawa, K. Radar Cross Section for Pedestrian in 76 GHz Band. *35th European Microwave Conference*, Paris, France, Vol.2, Oct. 2005.

Acronyms

ARL	U.S. Army Research Laboratory
CAD	computer-aided design
CEM	computational electromagnetics
CPU	central processing unit
DoD	Department of Defense
EM	electromagnetic
FDTD	Finite Difference Time Domain
GUI	graphics user interface
H-H	horizontal-horizontal
HPC	high-performance computing
MSRC	Major Shared Resource Center
PO	physical optics
RCS	radar cross section
RMS	root mean square
SAIC	Science Applications International Corporation
UWB	ultra-wideband
V-V	vertical-vertical

Distribution List

No. Copies	Organization
1elec	ADMNSTR DEFNS TECHL INFO CTR ATTN DTIC-OCP (ELECTRONIC COPY) 8725 JOHN J KINGMAN RD STE 0944 FT BELVOIR VA 22060-6218
1 HC	DARPA ATTN IXO S WELBY 3701 N FAIRFAX DR ARLINGTON VA 22203-1714
1 HC	OFC OF THE SECY OF DEFNS ATTN ODDRE (R&AT) THE PENTAGON WASHINGTON DC 20301-3080
1 HC	US ARMY RSRCH DEV AND ENGRG CMND ARMAMENT RSRCH DEV AND ENGRG CTR ARMAMENT ENGRG AND TECHNLGY CTR ATTN AMSRD-AAR-AEF-T J MATTS BLDG 305 ABERDEEN PROVING GROUND MD 21005-5001
1 HC	US ARMY TRADOC BATTLE LAB INTEGRATION & TECHL DIRCTRT ATTN ATCD-B 10 WHISTLER LANE FT MONROE VA 23651-5850
1 HC	PM TIMS, PROFILER (MMS-P) AN/TMQ-52 ATTN B GRIFFIES BUILDING 563 FT MONMOUTH NJ 07703
1 HC	SMC/GPA 2420 VELA WAY STE 1866 EL SEGUNDO CA 90245-4659
1 HC	US ARMY INFO SYS ENGRG CMND ATTN AMSEL-IE-TD F JENIA FT HUACHUCA AZ 85613-5300
1 HC	COMMANDER US ARMY RDECOM ATTN AMSRD-AMR W C MCCORKLE 5400 FOWLER RD REDSTONE ARSENAL AL 35898-5000
1 HC	US ARMY RDECOM CERDEC I2WD ATTN AMSRD-CER-IW-RA D THOMAS ATTN AMSRD-CER-IW-RA V FEDOROW BLDG 600 MCAFEE CTR FT MONMOUTH NJ 07703
1 HC	US ARMY RSRCH LAB ATTN AMSRD-ARL-CI-OK-TP TECHL LIB T LANDFRIED BLDG 4600 ABERDEEN PROVING GROUND MD 21005-5066
1 HC	US GOVERNMENT PRINT OFF DEPOSITORY RECEIVING SECTION ATTN MAIL STOP IDAD J TATE 732 NORTH CAPITOL ST., NW WASHINGTON DC 20402
1 HC	DIRECTOR US ARMY RSRCH LAB ATTN AMSRD-ARL-RO-EV W D BACH PO BOX 12211 RESEARCH TRIANGLE PARK NC 27709
11 HC	US ARMY RSRCH LAB ATTN AMSRD-ARL-CI-OK-T TECHL PUB (2 COPIES) ATTN AMSRD-ARL-CI-OK-TL TECHL LIB ATTN AMSRD-ARL-D J M MILLER ATTN AMSRD-ARL-SE-RM D WIKNER ATTN AMSRD-ARL-SE-RU A SULLIVAN ATTN AMSRD-ARL-SE-RU C LE ATTN AMSRD-ARL-SE-RU K KAPPRA ATTN AMSRD-ARL-SE-RU K RANNEY ATTN AMSRD-ARL-SE-RU T DOGARU ATTN IMNE-ALC-IMS MAIL & RECORDS MGMT ADELPHI MD 20783-1197

Total: 24 (1 Electronic, 23 HCS)

INTENTIONALLY LEFT BLANK